Matrix Isolation Infrared Spectroscopic and Theoretical Study of Nickel, Palladium, and Platinum Nitrous Oxide Complexes

Xi Jin, Guanjun Wang, and Mingfei Zhou*

Shanghai Key Laboratory of Molecular Catalysts and Innovative Materials, Department of Chemistry & Laser Chemistry Institute, Fudan University, Shanghai 200433, People's Republic of China

Received: March 13, 2006; In Final Form: April 27, 2006

Binary nickel, palladium, and platinum nitrous oxide complexes $Ni(NNO)_x$, $Pd(NNO)_x$ ($x = 1, 2$), and PtNNO have been produced by the reactions of laser-evaporated metal atoms with nitrous oxide in solid argon. The complexes were identified on the basis of isotopically substituted infrared absorptions as well as theoretical frequency calculations. These complexes were characterized to have structures with the terminal N atom of N_2O bound to the metal atoms. The MNNO complexes are photosensitive and rearrange to OMNN or $MO + N_2$ upon ultraviolet−visible irradiation.

Introduction

Nitrous oxide is a potent greenhouse gas with a global warming potential about 310 times that of CO_2 on a per molecule basis. It is the main source of stratospheric NO_x and contributes to stratospheric ozone depletion.[1] N_2O also acts as a potentially clean and highly selective oxygen donor for catalytic oxidation processes. Transition-metal-mediated N_2O activation and decomposition is of great current interest.[2] The reactions of gas-phase nitrous oxide with transition metals have been intensively studied both experimentally and theoretically,[3−19] which may serve as the simplest model in understanding the intrinsic mechanism of the catalytic reduction processes.

The reactions of transition-metal atoms with N_2O leading to N−O bond activation to form the metal oxide and N_2 are quite exothermic. However, most of these reactions are inefficient even at room temperature, indicating the presence of energy barriers.[3,4] Matsui et al. have reported experimental data of depletion kinetics of Ni atoms by N_2O at room temperature.[6] It was found that no depletion was observed for the ground state of the Ni atom. The first low-lying excited state of Ni (a^3D) ($3d^94s^1$ configuration) also showed inefficient depletion. However, the depletion became efficient with increasing electronic energy. Campbell and co-workers have reported gas-phase kinetic studies on the reactivity of Ni, Pd, and Pt atoms with N_2O as a function of temperature and pressure.[10,11] It has been determined that all three metals exhibited pressure-dependent kinetics with N_2O, indicating adduct formation. Both nickel and platinum exhibited an abstraction channel with a barrier, but palladium did not.

Different mechanisms have been proposed to account for the kinetics of the reactions of transition-metal atoms with N_2O.[3,7,13] Theoretical calculations suggest that the reactions proceed via the initial formation of an encounter weak complex before the transition state.[14,19] However, no binary transition-metal nitrous oxide complex has been experimentally characterized. Nitrous oxide is generally regarded as a "poor" ligand, and only very few transition-metal complexes containing the nitrous oxide ligand have been characterized.[20−23] Recently, copper and silver chloride−nitrous oxide complexes, ClCuNNO and ClAgNNO, have been produced and trapped in solid argon by the reactions of metal chlorides with nitrous oxide in solid argon. These complexes were characterized to have linear structures with the terminal N atom of N_2O being bound to the metal atoms.[24]

In this paper, we report a matrix isolation infrared spectroscopic and theoretical study of binary unsaturated nickel, palladium, and platinum nitrous oxide complexes, which were produced by the reactions of metal atoms with nitrous oxide in solid argon.

Experimental and Theoretical Methods

The experimental setup for pulsed laser ablation and matrix isolation infrared absorption spectroscopic investigation has been described in detail previously.[25] Briefly, the 1064 nm Nd:YAG laser fundamental (Spectra Physics, DCR 2, 20 Hz repetition rate and 8 ns pulse width) was focused onto the rotating metal target through a hole in a CsI window. The laser-evaporated metal atoms were codeposited with N_2O in excess argon onto the 12 K CsI window. The CsI window was mounted on a copper holder at the cold end of the cryostat (Air Products Displex DE202) and maintained by a closed-cycle helium refrigerator (Air Products Displex IR02W). In general, matrix samples were deposited for 1−2 h with a gas deposition rate of approximately 4 mmol/h. A Bruker IFS 113v Fourier transform infrared spectrometer equipped with a DTGS detector was used to record the IR spectra in the range of 4000−400 cm^{-1} with a resolution of 0.5 cm^{-1}. The N_2O/Ar mixtures were prepared in a stainless steel vacuum line using the standard manometric technique. Nitrous oxide (Shanghai BOC, 99.99%), isotopically labeled $^{15}N_2O$ (Cambridge Isotope Laboratory, 99%), and $^{15}N_2O + {}^{14}N_2O$ mixtures were used in different experiments.

Density functional calculations were performed using the Gaussian 03 program.[26] The most popular Becke three-parameter hybrid functional, with additional correlation corrections due to Lee, Yang, and Parr, was utilized (B3LYP).[27] This hybrid functional can provide reliable predictions of the state energies, structures, and vibrational frequencies of transition-metal-containing compounds.[28] The 6-311+G* basis set for N and O atoms, the all-electron basis set of Wachters−Hay as modified by Gaussian for Ni, and the SDD pseudopotential and basis set

* To whom correspondence should be addressed. E-mail: mfzhou@fudan.edu.cn.

10.1021/jp061557p CCC: $33.50
Published on Web 06/15/2006

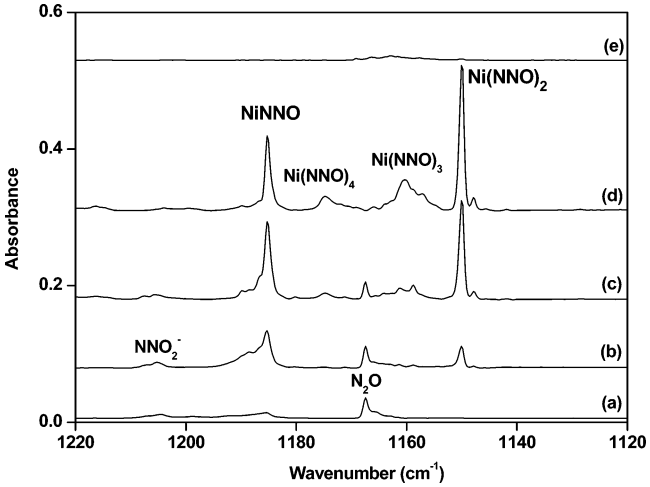

Figure 1. Infrared spectra in the 1220−1120 cm^{-1} region from codeposition of laser-evaporated Ni atoms with 0.2% N_2O in argon: (a) 1 h of sample deposition at 12 K, (b) after annealing to 25 K, (c) after annealing to 30 K, (d) after annealing to 40 K, and (e) after 15 min of broad-band irradiation.

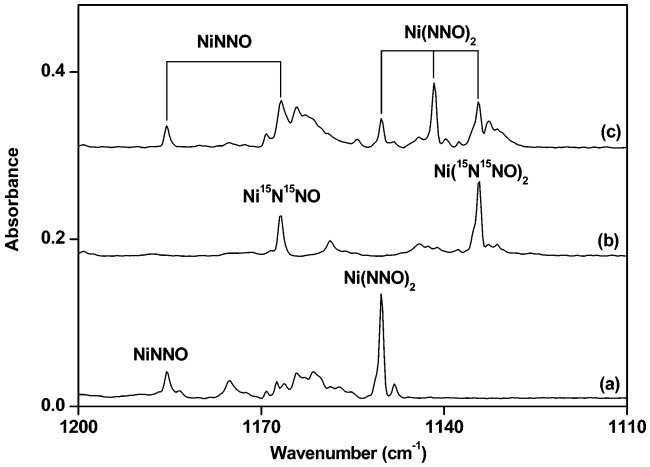

Figure 2. Infrared spectra in the 1200−1110 cm^{-1} region from codeposition of laser-evaporated Ni atoms with N_2O in excess argon. Spectra were taken after 1 h of sample deposition followed by 35 K annealing: (a) 0.2% $^{14}N_2O$, (b) 0.2% $^{15}N_2O$, and (c) 0.2% $^{14}N_2O$ + 0.2% $^{15}N_2O$.

for Pd and Pt were used.[29,30] The geometries were fully optimized, and the vibrational frequencies were calculated with analytic second derivatives, and zero-point vibration energies (ZPVEs) were derived. Basis set superposition errors were also corrected.

Results and Discussion

Infrared Spectra. Experiments were done for laser-evaporated Ni, Pd, and Pt atom reactions with N_2O in excess argon using different laser energies and N_2O concentrations. After sample deposition, strong N_2O fundamentals and weak overtone and combination absorptions were presented.[31] Weak absorptions at 1353.8, 1204.9, and 1007.3 cm^{-1} were also observed on sample deposition, decreased on subsequent annealing to higher temperature, and disappeared when the sample was subjected to broad-band irradiation with the high-pressure mercury arc lamp (250 nm < λ < 580 nm). These absorptions are common for different metals and correspond to the absorptions reported at 1355, 1205.5, and 1008 cm^{-1} that were previously assigned to the NNO_2^- anion.[32] Weak metal-independent absorptions at 1776.0 and 1863.2 cm^{-1} were produced on broad-band irradiation, during which the NNO_2^- anion absorptions were destroyed. These two absorptions are due to the symmetric and antisymmetric N−O stretching vibrations of the *cis*-$(NO)_2$ complex.[33]

Infrared spectra in the N−O stretching frequency region using a nickel target with 0.2% N_2O in argon are shown in Figure 1, and the product absorptions are listed in Table 1. Besides the above-mentioned absorptions, a new absorption at 1185.5 cm^{-1} was also observed on sample deposition. This band increased step-by-step on subsequent sample annealing to higher temperatures (Figure 1, traces b−d). On sample annealing to 25 K, a new absorption at 1150.3 cm^{-1} was produced, which increased markedly on higher temperature annealing, during which weak absorptions at 1160.4 and 1174.8 cm^{-1} were also produced. These bands were destroyed when the sample was subjected to broad-band irradiation (Figure 1, trace e), during which weak absorptions at 825.1 and 822.2 cm^{-1} (not shown) were produced. The relative intensities of the 825.1 and 822.2 cm^{-1} absorptions remained constant through all the experiments and match the natural abundance of Ni (^{58}Ni, 68%; ^{60}Ni, 26%). These two bands are due to the ^{58}NiO and ^{60}NiO absorptions, which were previously reported at 825.7 and 822.8 cm^{-1} in solid argon.[34] In the experiments with relatively higher laser energy, weak absorptions due to NiNN (2089.2 cm^{-1}) were also observed on sample annealing.[35] The experiments were repeated using the isotopically labeled $^{15}N_2O$ sample and the $^{14}N_2O$ + $^{15}N_2O$ mixture. The spectra in the 1200−1110 cm^{-1} region with different samples are shown in Figure 2, and the isotopic absorptions are listed in Table 1.

TABLE 1: Infrared Absorptions (cm^{-1}) from Codeposition of Laser-Evaporated Ni, Pd, and Pt Atoms with N_2O in Excess Argon

$^{14}N_2O$	$^{15}N_2O$	$^{14}N_2O + {}^{15}N_2O$	assignment
2218.5	2149.5		N_2O N−N str
1282.7	1263.1		N_2O N−O str
1185.5	1167.5	1185.5, 1167.5	NiNNO N−O str
1150.3	1134.4	1150.3, 1141.6, 1134.4	$Ni(NNO)_2$ asym N−O str
1160.4	1144.0		$Ni(NNO)_3$ asym N−O str
1174.8	1158.5		$Ni(NNO)_4$ asym N−O str
825.1	825.1		^{58}NiO
822.2	822.2		^{60}NiO
1226.8	1209.4	1226.8, 1209.4	PdNNO N−O str
2254.2	2186.0	−	$Pd(NNO)_2$ asym N−N str
2257.6	−	−	$Pd(NNO)_2$ site
1226.3	1209.2	1226.3, 1215.9, 1209.4	$Pd(NNO)_2$ asym N−O str
1230.4	1213.3	1230.4, 1220.2, 1213.3	$Pd(NNO)_2$ site
2267.9	2194.1		PtNNO N−N str
1229.4	1210.9	1229.4, 1210.9	PtNNO N−O str
827.5	827.5		PtO

Similar experiments were performed using a palladium target. The spectra in the N−N and N−O stretching frequency regions from codeposition of laser-evaporated palladium atoms with 0.2% N_2O in argon are illustrated in Figure 3. A new product absorption at 1226.8 cm^{-1} appeared on sample annealing to 25 K. As can be seen, the 1226.8 cm^{-1} band increased on subsequent higher temperature annealing, but the band shape became asymmetric and the peak position shifted to 1226.3 cm^{-1}. New absorptions at 2257.6, 2254.2, and 1230.4 cm^{-1} were also observed to increase on sample annealing. Broad-band irradiation bleached these product absorptions. When a 0.2% $^{15}N_2O$ sample was used, all the above-mentioned product absorptions were shifted with the frequencies listed in Table 1. The spectra in the 1240−1200 cm^{-1} region using a mixed 0.2% $^{14}N_2O$ + 0.2% $^{15}N_2O$ sample are shown in Figure 4.

The spectra in the N−N and N−O stretching frequency regions from codeposition of laser-evaporated platinum atoms

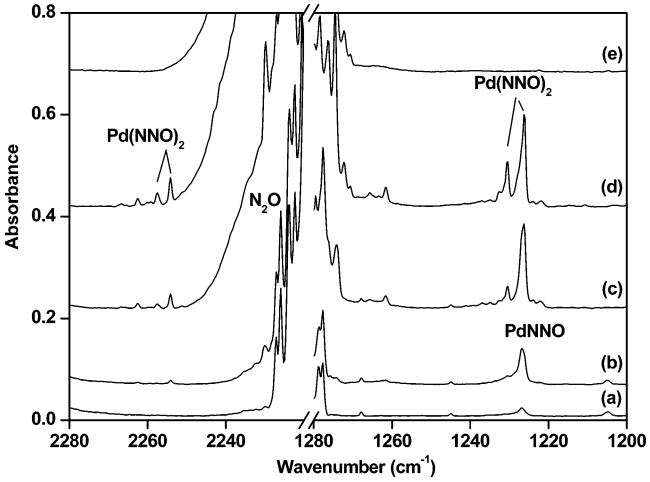

Figure 3. Infrared spectra in the 2270−2220 and 1250−1200 cm^{-1} regions from codeposition of laser-evaporated Pd atoms with 0.2% N_2O in argon: (a) 1 h of sample deposition at 12 K, (b) after annealing to 25 K, (c) after annealing to 35 K, (d) after annealing to 40 K, (e) after 20 min of broad-band irradiation.

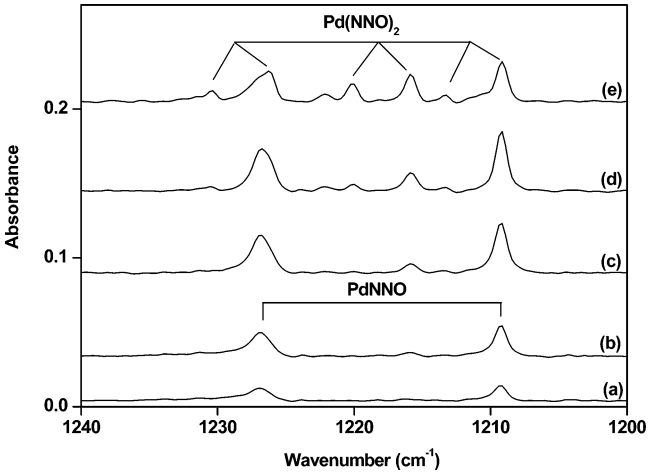

Figure 4. Infrared spectra in the 1240−1200 cm^{-1} region from codeposition of laser-evaporated Pd atoms with 0.2% $^{14}N_2O$ + 0.2% $^{15}N_2O$ in argon: (a) 1 h of sample deposition at 12 K, (b) after annealing to 25 K, (c) after annealing to 30 K, (d) after annealing to 35 K, and (e) after annealing to 40 K.

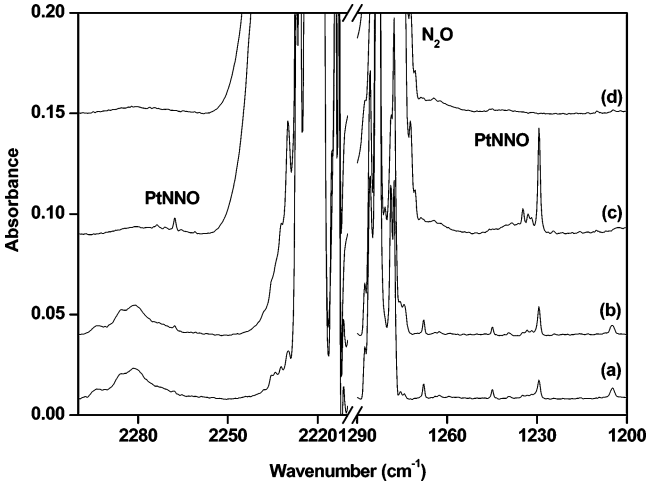

Figure 5. Infrared spectra in the 2300−2210 and 1290−1200 cm^{-1} regions from codeposition of laser-evaporated Pt atoms with 0.2% N_2O in argon: (a) 1 h of sample deposition at 12 K, (b) after annealing to 25 K, (c) after annealing to 38 K, and (d) after 20 min of broad-band irradiation.

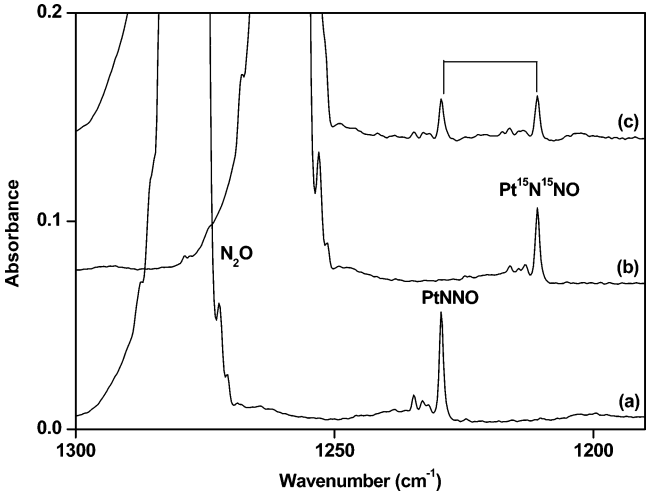

Figure 6. Infrared spectra in the 1300−1190 cm^{-1} region from codeposition of laser-evaporated Pt atoms with isotopically labeled N_2O in excess argon: (a) 0.2% $^{14}N_2O$, (b) 0.2% $^{15}N_2O$, and (c) 0.2% $^{14}N_2O$ + 0.2% $^{15}N_2O$. Spectra were taken after 1 h of sample deposition followed by 38 K annealing.

with 0.2% N_2O in argon are shown in Figure 5. New product absorptions were observed at 2267.9 and 1229.4 cm^{-1} after sample deposition and increased together on sample annealing. Both bands disappeared upon broad-band irradiation, during which a weak band at 827.5 cm^{-1} (not shown) was produced. The 827.5 cm^{-1} band is due to PtO absorption, which was reported at 828 cm^{-1} in solid argon.[36] The isotopic shift and splitting for the 1229.4 cm^{-1} band with $^{15}N_2O$ and the $^{14}N_2O$ + $^{15}N_2O$ mixture are illustrated in Figure 6.

Ni(NNO)$_x$. The absorption at 1185.5 cm^{-1} in the Ni + N_2O/Ar reaction is assigned to the NiNNO molecule. It shifted to 1167.5 cm^{-1} with the $^{15}N_2O$ sample. The $^{14}N/^{15}N$ isotopic frequency ratio of 1.0154 is about the same as that of the N−O stretching mode of N_2O (1.0155) observed at 1282.7 cm^{-1} in solid argon. The band position and isotopic frequency ratio indicate that this band is due to a N−O stretching vibration of a nitrous oxide complex. In the mixed $^{14}N_2O$ + $^{15}N_2O$ experiment (Figure 2), only the pure isotopic counterparts were observed, indicating that only one N_2O is involved in this mode.

Density functional calculations were performed to support the assignment. Two possible geometric NiN_2O isomers, namely, a η^1-N-bonded NiNNO complex and a η^1-O-bonded NiONN complex, were considered. The NiNNO complex was predicted to have a singlet ground state with a linear structure (Figure 7). The lowest triplet state of NiNNO is bent with ∠NiNN = 133.9°. This state lies 5.0 kcal/mol above the singlet ground state. The NiONN complex has a triplet ground state with a bent structure with a quite long Ni−O distance, in agreement with the previous calculations.[14] Geometry optimization on the singlet state of the NiONN complex converged to the inserted ONiNN structure. At the B3LYP/6-311+G* level of theory, the singlet NiNNO structure is 7.5 kcal/mol lower in energy than the triplet-state NiONN isomer. As listed in Table 2, the singlet ground state of the NiNNO complex was predicted to have two intense IR absorptions at 1265.7 and 2336.5 cm^{-1} with 688:89 km/mol relative intensities. The upper band is due to the N−N stretching vibration, and the low band is due to the N−O stretching mode. The predicted N−O stretching frequency is 6.3% higher than the experimental value. The N−N stretching mode was predicted to be 8.1 cm^{-1} lower than that of N_2O calculated at the same level of theory. This mode is overlapped by the N_2O absorption. The N−N stretching mode of N_2O

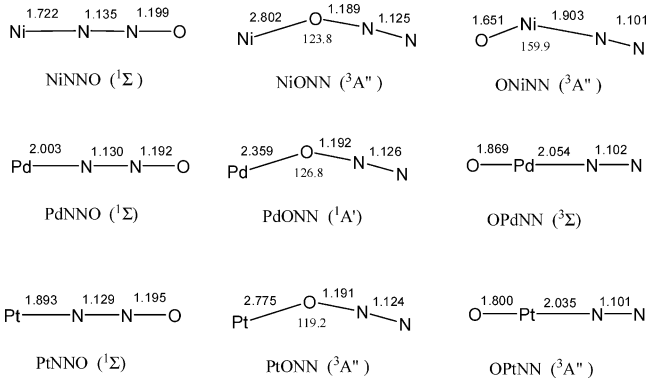

Figure 7. Optimized structures (bond lengths in angstroms and bond angles in degrees) of the MN_2O (M = Ni, Pd, Pt) isomers.

TABLE 2: Calculated Total Energies (hartrees, after Zero-Point Energy Correction), Vibrational Frequencies (cm^{-1}), and Intensities (km/mol, in Parentheses) of Various Species in the Ni, Pd, and Pt + N_2O Systems

	energy	N−N str	N−O str	M═O
N_2O ($^1\Sigma$)	−184.70722	2344.6 (401)	1327.7 (69)	
NiNNO ($^1\Sigma$)	−1692.96733	2336.5 (89)	1265.7 (688)	
NiNNO ($^3A''$)	−1692.96178	2243.1 (233)	1253.1 (558)	
NiONN ($^3A''$)	−1692.95742	2336.4 (511)	1306.9 (77)	
ONiNN ($^3A''$)	−1693.04964	2364.4 (281)		812.6 (5)
$Ni(NNO)_2$ ($^1\Sigma_g$)	−1877.72592	2352.6 (0)	1317.8 (0)	
		2351.0 (348)	1251.7 (1904)	
$Ni(NNO)_3$ ($^1A_1$)	−2062.43883	2328.2 (438)	1239.4 (2463)	
$Ni(NNO)_4$ ($^1A_1$)	−2247.14637	2344.2 (0)	1313.5 (0)	
		2331.3 (648)	1243.1 (2848)	
PdNNO ($^1\Sigma$)	−312.61625	2340.6 (172)	1277.5 (464)	
PdONN (^1A)	−312.59778	2322.6 (613)	1281.7 (32)	
OPdNN ($^3\Sigma$)	−312.63953	2357.8 (259)		582.0 (7)
$Pd(NNO)_2$ ($^1\Sigma_g$)	−497.35370	2370.7 (0)	1318.2 (0)	
		2369.5 (507)	1275.3 (1373)	
PtNNO ($^1\Sigma$)	−304.04280	2395.1 (164)	1285.7 (526)	
PtONN (^3A)	−304.01168	2339.1 (481)	1303.5 (95)	
OPtNN ($^3\Sigma$)	−304.10847	2349.1 (196)		758.4 (0)
$Pt(NNO)_2$ ($^1\Sigma_g$)	−488.80330	2409.0 (0)	1329.4 (0)	
		2407.9 (526)	1275.2 (1598)	

observed at 2218.5 cm^{-1} is very strong and broad, particularly after sample annealing.

The 1150.3 cm^{-1} absorption appeared after the NiNNO absorption. This band is favored in the experiments with relatively high N_2O concentrations with respect to NiNNO. It shifted to 1134.4 cm^{-1} with $^{15}N_2O$. The band position and isotopic frequency ratio (1.0140) suggest that this band is due to the N−O stretching mode of a nitrous oxide complex. When the mixed 0.2% $^{14}N_2O$ + 0.2% $^{15}N_2O$ sample was used, a triplet at 1150.3, 1141.6, and 1134.4 cm^{-1} with approximately 1:2:1 relative intensities was observed, which indicates that two equivalent N_2O subunits are involved in this mode. Accordingly, we assign the 1150.3 cm^{-1} band to the antisymmetric N−O stretching mode of the $Ni(NNO)_2$ complex. The observation of only one IR absorption suggests that the complex is linear or near linear.

The assignment is supported by density functional calculations. The $Ni(NNO)_2$ complex was predicted to have a singlet ground state with a linear structure (Figure 8). The antisymmetric N−O stretching mode was predicted at 1251.7 cm^{-1}. The antisymmetric N−N stretching mode is also IR active and was predicted at 2351.0 cm^{-1}. This mode is only about 6.4 cm^{-1} higher than that of the N_2O molecule and is overlapped by the strong N_2O absorption.

The 1160.4 and 1174.8 cm^{-1} absorptions also exhibited N−O stretching vibrational ratios (1.0143 and 1.0141). These bands

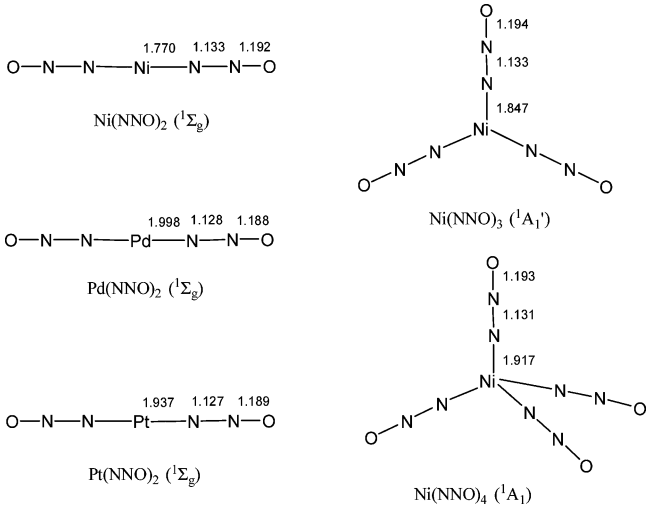

Figure 8. Optimized structures (bond lengths in angstroms and bond angles in degrees) of the $M(NNO)_2$ (M = Ni, Pd, Pt), $Ni(NNO)_3$, and $Ni(NNO)_4$ complexes.

appeared after the $Ni(NNO)_2$ absorption and are tentatively assigned to the $Ni(NNO)_3$ and $Ni(NNO)_4$ complexes. The $Ni(NNO)_3$ complex was predicted to have a planar D_{3h} structure (Figure 8) with a doubly degenerated N−O stretching mode at 1239.4 cm^{-1}. The binding energy of the third N_2O was estimated to be 2.8 kcal/mol. The $Ni(NNO)_4$ molecule was predicted to have a tetrahedral (T_d) structure with a triply degenerated N−O stretching mode at 1243.1 cm^{-1}. The fourth N_2O was predicted to be bound by only 0.2 kcal/mol without basis set superposition error corrections. This value becomes positive after basis set superposition error corrections.

$Pd(NNO)_x$. The absorption at 1226.8 cm^{-1} in the Pd + N_2O experiments is assigned to the PdNNO complex following the example of NiNNO. This band shifted to 1209.4 cm^{-1} with $^{15}N_2O$, and only the pure isotopic counterparts were observed in the mixed $^{14}N_2O$ + $^{15}N_2O$ experiment. As shown in Figure 7, the PdNNO complex was predicted to have a singlet ground state with a linear structure. The N−O stretching mode was computed at 1277.5 cm^{-1}, which is about 4.0% higher than the observed value. The N−N stretching mode was predicted at 2340.6 cm^{-1}, just 4 cm^{-1} lower than that of the N_2O molecule calculated at the same level of theory. This mode is overlapped by the strong N_2O absorption.

Absorptions at 1226.3/1230.4 and 2254.2/2257.6 cm^{-1} are assigned to the N−O and N−N stretching modes of the $Pd(NNO)_2$ complex in different matrix sites. The 1226.3 cm^{-1} band exhibits the same isotopic frequency ratio as the 1230.4 cm^{-1} band (1.0141). In the experiment with the mixed 0.2% $^{14}N_2O$ + 0.2% $^{15}N_2O$ sample (Figure 4), the 1226.3 cm^{-1} band splits into a triplet with an intermediate at 1215.9 cm^{-1}. A similar triplet with an intermediate at 1220.2 cm^{-1} was also observed for the 1230.4 cm^{-1} band. The antisymmetric N−N and N−O stretching modes of the linear singlet ground-state $Pd(NNO)_2$ molecule were computed at 2369.5 and 1275.3 cm^{-1}, respectively.

No evidence was found for the formation of the $Pd(NNO)_3$ and $Pd(NNO)_4$ complexes in the present experiments. Both the $Pd(CO)_3$ and $Pd(CO)_4$ carbonyl complexes have been trapped in solid matrixes.[37] However, the $Pd(NNO)_3$ molecule was predicted to be unbound with respect to $Pd(NNO)_2$ + N_2O and, therefore, cannot be formed via the $Pd(NNO)_2$ + N_2O reaction.

PtNNO. The 1229.4 and 2267.9 cm^{-1} absorptions are the only new product absorptions observed in the Pt + N_2O

experiments. The upper band shifted to 2194.1 cm^{-1} with $^{15}N_2O$. The $^{14}N/^{15}N$ isotopic frequency ratio of 1.0336 indicates that this band is due to a N−N stretching mode. The low band shifted to 1210.9 cm^{-1} with $^{15}N_2O$, giving a $^{14}N/^{15}N$ ratio of 1.0153. The band positions and isotopic frequency ratios are appropriate for the N−N and N−O stretching modes of a nitrous oxide complex. The mixed $^{14}N_2O + {}^{15}N_2O$ spectrum (Figure 6) clearly shows that only one N_2O subunit is involved in the complex. Therefore, we assign the 1229.4 and 2267.9 cm^{-1} bands to the N−O and N−N stretching vibrations of the PtNNO complex. The PtNNO complex also was predicted to have a singlet ground state with a linear structure. The N−N and N−O stretching vibrations were calculated at 2395.1 and 1285.7 cm^{-1} with 164: 526 km/mol relative IR intensities, which are in quite good agreement with the experimental values.

No evidence was found for the formation of higher platinum nitrous oxide complexes. The $Pt(NNO)_2$ molecule was predicted to have a linear singlet ground state and is more stable than PtNNO + N_2O by about 32.5 kcal/mol. It has two intense IR absorptions at 1275.2 cm^{-1} (1598 km/mol) and 2407.9 cm^{-1} (526 km/mol). The $Pt(NNO)_3$ molecule was predicted to be unstable with respect to $Pt(NNO)_2 + N_2O$.

Bonding Mechanism. The bonding interactions between metal and nitrous oxide in metal nitrous oxide complexes can be described as the synergic donation of electrons in the HOMO of N_2O to an empty σ orbital of the metal and the back-donation of the metal π electrons to the LUMO orbital of N_2O. The ground-state N_2O molecule has an electron configuration of $(1\sigma)^2(2\sigma)^2(3\sigma)^2(4\sigma)^2\ (5\sigma)^2(6\sigma)^2(1\pi)^4(7\sigma)^2(2\pi)^4(3\pi)^0$. The highest occupied 2π orbital is antibonding with respect to the N−O bond but bonding for the N−N bond. The highest occupied σ orbital (7σ) is predominantly N−N σ antibonding in character. The LUMO is a 3π orbital with antibonding character for both the N−N and N−O bonds. In the linear MNNO structure, the 7σ orbital of N_2O is the principal donor orbital, while the 2π orbital is less important in donation because of charge accumulation in the N−N midbond region. The donation interaction between the 7σ orbital of N_2O and a vacant metal orbital with σ symmetry stabilizes the M−N and N−N bonds, while the back-donation from the metal dπ orbital to the 3π antibonding orbital of N_2O destabilizes both the N−N and N−O bonds. Consistent with this notion, the N−O stretching frequencies of the above-characterized nitrous oxide complexes are red-shifted, while the N−N stretching frequencies are either blue-shifted (Pt) or about the same (Ni and Pd, by calculation) when compared to the N_2O frequencies. The nickel complexes have the lowest N−O stretching frequencies, which suggests that nickel has the largest back-donation. The N−O stretching frequencies of PdNNO and PtNNO are about the same, but the N−N stretching frequency of PtNNO is higher than that of PdNNO, indicating that there are more donations in PtNNO than that in PdNNO. These differences can be understood on the basis of the energy differences between the valence $(n-1)$d and ns orbitals of the metal atoms, as has been discussed for the transition-metal carbonyls and thiocarbonyls of group 12 metals.[38,39]

Reaction Mechanism. The above-characterized metal nitrous oxide complexes were formed by the reactions of ground-state metal atoms and nitrous oxide in solid argon. These association reactions are exothermic and require negligible activation energy.

$$Ni\ (^3D) + N_2O\ (^1\Sigma) \rightarrow NiNNO\ (^1\Sigma)\ (\Delta E = -7.4\ \text{kcal/mol}) \quad (1)$$

$$NiNNO\ (^1\Sigma) + N_2O\ (^1\Sigma) \rightarrow Ni(NNO)_2\ (^1\Sigma_g)\ (\Delta E = -31.0\ \text{kcal/mol}) \quad (2)$$

$$Pd\ (^1S) + N_2O\ (^1\Sigma) \rightarrow PdNNO\ (^1\Sigma)\ (\Delta E = -13.7\ \text{kcal/mol}) \quad (3)$$

$$PdNNO\ (^1\Sigma) + N_2O\ (^1\Sigma) \rightarrow Pd(NNO)_2\ (^1\Sigma_g)\ (\Delta E = -18.1\ \text{kcal/mol}) \quad (4)$$

$$Pt\ (^3D) + N_2O\ (^1\Sigma) \rightarrow PtNNO\ (^1\Sigma)\ (\Delta E = -20.2\ \text{kcal/mol}) \quad (5)$$

The $^1\Sigma$ ground-state MNNO complexes correlate with the $(n-1)d^{10}ns^0$ electron configuration of the metal atoms. Ni has a ^3F ground state derived from the $3d^84s^2$ configuration, but a ^3D level with $3d^94s^1$ configuration lies approximately 250 cm^{-1} higher in energy than the ^3D level. At the annealing temperatures (25−40 K), the ^3D level is populated. The formation of singlet NiNNO involves nickel 4s to 3d promotion. Since there are two N_2O molecules to share the cost of 4s to 3d promotion, the binding energy of the second N_2O (31.0 kcal/mol) is significantly higher than that of the first N_2O (7.4 kcal/mol).

The $M(NNO)_x$ complex absorptions were destroyed on-broad band irradiation. The MNNO complexes are expected to be rearranged to the OMNN isomer or MO + N_2. As can be seen in Table 2, all three OMNN complexes were predicted to have triplet ground states. The ONiNN molecule is bent, while the OPdNN and OPtNN molecules are linear. The OMNN inserted isomer is more stable than the MNNO complex; therefore, the isomerization reactions are exothermic but require activation energies. The M−O stretching modes of these insertion molecules were predicted to have very low IR intensities, while the N−N stretching modes were predicted to be very close to the N−N stretching mode of N_2O. Therefore, these insertion molecules cannot be observed in the present experiments. However, both NiO and PtO were observed upon broad-band irradiation. Due to the unique closed-shell (d^{10}) configuration of the palladium atom, PdO has an unusually small bond energy and has not been observed in solid noble gas matrixes.[36,40]

Conclusions

Nickel, palladium, and platinum nitrous oxide complexes $Ni(NNO)_{1-2}$, $Pd(NNO)_{1-2}$, and PtNNO have been studied by matrix isolation infrared absorption spectroscopy and density functional theory calculations. These metal nitrous oxide complexes were produced by the reactions of metal atoms and nitrous oxide molecules in a solid argon matrix and were characterized to have structures with the terminal N atom of N_2O bound to the metal atoms. The bonding in these nitrous oxide complexes involves the synergic donation of electrons in 7σ of N_2O to an empty symmetry-matching orbital of the metal and the back-donation of the metal π electrons to the N_2O $3\pi^*$ orbital, which induces a blue shift of the N−O stretching vibrational frequencies. The MNNO complexes are photosensitive and rearrange to OMNN or MO + N_2 upon ultraviolet−visible irradiation.

Acknowledgment. We gratefully acknowledge financial support from the National Natural Science Foundation of China (Grant Nos. 20125311 and 20203005).

References and Notes

(1) Dickinson, R. E.; Cicerone, R. J. *Nature* **1986**, 109. Thiemans, M. H.; Trogler, W. C. *Science* **1991**, *251*, 932. Trogler, W. C. *Coord. Chem. Rev.* **1999**, *187*, 303.

(2) Kapteijn, F.; Rodriguez-Mirasol, J.; Moulijn, J. A. *Appl. Catal., B* **1996**, *9*, 25. Dandekar, A.; Vannice, M. A. *Appl. Catal., B* **1999**, *22*, 179. Burch, R.; Daniells, S. T.; Breen, J. P.; Hu, P. *J. Catal.* **2004**, *224*, 252.

(3) Ritter, D.; Weisshaar, J. C. *J. Phys. Chem.* **1990**, *94*, 4907. Ritter, D.; Weisshaar, J. C. *J. Phys.* Chem. **1989**, *93*, 1576.

(4) Plane, J. M. C.; Rollason, R. J. *J. Chem. Soc., Faraday Trans.* **1996**, *92*, 4371.

(5) Clemmer, D. E.; Honma, K.; Koyano, I. *J. Phys. Chem.* **1993**, *97*, 11480.

(6) Matsui, R.; Senba, K.; Honma, K. *J. Phys. Chem. A* **1997**, *101*, 179.

(7) Campbell, M. L.; McClean, R. E. *J. Phys. Chem.* **1993**, *97*, 7942. Campbell, M. L.; McClean, R. E. *J. Chem. Soc., Faraday Trans*. **1995**, *91*, 3787.

(8) Campbell, M. L. *J. Chem. Phys.* **1996**, *104*, 7515. Campbell, M. L.; Hooper, K. L. *J. Chem. Soc., Faraday Trans*. **1997**, *93*, 2139.

(9) Campbell, M. L. Hooper, K. L.; Kolsch, E. J. *Chem. Phys. Lett.* **1997**, *274*, 7. Campbell, M. L. *Chem. Phys. Lett.* **1998**, *294*, 339.

(10) Campbell, M. L.; Kolsch, E. J.; Hooper, K. L. *J. Phys. Chem. A* **2000**, *104*, 11147.

(11) Campbell, M. L. *J. Chem. Soc., Faraday Trans.* **1998**, *94*, 353. Campbell, M. L. *J. Phys. Chem. A* **2003**, *107*, 3048.

(12) Armentrout, P. B.; Halle, L. F.; Beauchamp, J. L. *J. Chem. Phys.* **1982**, *76*, 2449. Rodgers, M. T.; Walker, B.; Armentrout, P. B. *Int. J. Mass Spectrom.* **1999**, *182/183*, 99.

(13) Futerko, P. M.; Fontijn, A. *J. Chem. Phys.* **1991**, *95*, 8065.

(14) Delabie, A.; Vinckier, C.; Flock, M.; Pierloot, K. *J. Phys. Chem. A* **2001**, *105*, 5479.

(15) Delabie, A.; Pierloot, K. *J. Phys. Chem. A* **2002**, *106*, 5679.

(16) Stirling, A. *J. Phys. Chem. A* **1998**, *102*, 6565. Stirling, A. *J. Am. Chem. Soc*. **2002**, *124*, 4058.

(17) Kryachko, E. S.; Tishchenko, O.; Nguyen, M. T. *Int. J. Quantum Chem.* **2002**, *89*, 329. Tishchenko, O.; Vinckier, C.; Nguyen, M. T. *J. Phys. Chem. A* **2004**, *108*, 1268. Tishchenko, O.; Vinckier, C.; Ceulemans, A.; Nguyen, M. T. *J. Phys. Chem. A* **2005**, *109*, 6099.

(18) Koyanagi, G. K.; Böhme, D. K. *J. Phys. Chem. A* **2001**, *105*, 8964. Lavrov, V. V.; Blagojevic, V.; Koyanagi, G. K.; Orlova, G.; Böhme, D. K. *J. Phys. Chem. A* **2004**, *108*, 5610. Blagojevic, V.; Orlova, G.; Böhme, D. K. *J. Am. Chem. Soc*. **2005**, *127*, 3545.

(19) Michelini, M. D.; Russo, N.; Alikhani, M. E.; Silvi, B. *J. Comput. Chem.* **2005**, *26*, 1284.

(20) Armor, J. N.; Taube, H. *J. Am. Chem. Soc.* **1969**, *91*, 6874. Armor, J. N.; Taube, H. *Chem. Commun.* **1971**, 287.

(21) Groves, J. T.; Roman, J. S. *J. Am. Chem. Soc.* **1995**, *117*, 5594.

(22) Pamplin, C. B.; Ma, E. S. F.; Safari, N.; Rettig, S. J.; James, B. R. *J. Am. Chem. Soc.* **2001**, *123*, 8596.

(23) Paulat, F.; Kuschel, T.; Nather, C.; Praneeth, V. K. K.; Sander, O.; Lehnert, N. *Inorg. Chem.* **2004**, *43*, 6979.

(24) Wang, G. J.; Jin, X.; Chen, M. H.; Zhou, M. F. *Chem. Phys. Lett.* **2006**, *420*, 130.

(25) Chen, M. H.; Wang, X. F.; Zhang, L. N.; Yu, M.; Qin, Q. Z. *Chem. Phys.* **1999**, *242*, 81;

(26) Frisch, M. J.; Trucks, G. W.; Schlegel, H. B.; Scuseria, G. E.; Robb, M. A.; Cheeseman, J. R.; Montgomery, J. A. J.; Vreven, T.; Kudin, K. N.; Burant, J. C.; Millam, J. M.; Iyengar, S. S.; Tomasi, J.; Barone, V.; Mennucci, B.; Cossi, M.; Scalmani, G.; Rega, N.; Petersson, G. A.; Nakatsuji, H.; Hada, M.; Ehara, M.; Toyota, K.; Fukuda, R.; Hasegawa, J.; Ishida, M.; Nakajima, T.; Honda, Y.; Kitao, O.; Nakai, H.; Klene, M.; Li, X.; Knox, J. E.; Hratchian, H. P.; Cross, J. B.; Adamo, C.; Jaramillo, J.; Gomperts, R.; Stratmann, R. E.; Yazyev, O.; Austin, A. J.; Cammi, R.; Pomelli, C.; Ochterski, J. W.; Ayala, P. Y.; Morokuma, K.; Voth, G. A.; Salvador, P.; Dannenberg, J. J.; Zakrzewski, V. G.; Dapprich, S.; Daniels, A. D.; Strain, M. C.; Farkas, O.; Malick, D. K.; Rabuck, A. D.; Raghavachari, K.; Foresman, J. B.; Ortiz, J. V.; Cui, Q.; Baboul, A. G.; Clifford, S.; Cioslowski, J.; Stefanov, B. B.; Liu, G.; Liashenko, A.; Piskorz, P.; Komaromi, I.; Martin, R. L.; Fox, D. J.; Keith, T.; Al-Laham, M. A.; Peng, C. Y.; Nanayakkara, A.; Challacombe, M.; Gill, P. M. W.; Johnson, B.; Chen, W.; Wong, M. W.; Gonzalez, C.; Pople, J. A. *Gaussian 03*, Revision B.05; Gaussian, Inc.: Pittsburgh, 2003.

(27) Becke, A. D. *J. Chem. Phys.* **1993**, *98*, 5648. Lee, C.; Yang, E.; Parr, R. G. *Phys. Rev. B* **1988**, *37*, 785.

(28) Bauschlicher, C. W., Jr.; Ricca, A.; Partridge, H.; Langhoff, S. R. In *Recent Advances in Density Functional Theory*; Chong, D. P., Ed.; World Scientific Publishing: Singapore, 1997; Part II. Siegbahn, P. E. M. *Electronic Structure Calculations for Molecules Containing Transition Metals*; Advances in Chemical Physics XCIII; Wiley: New York, 1996. Bytheway, I.; Wong, M. W. *Chem. Phys. Lett*. **1998**, *282*, 219.

(29) McLean, A. D.; Chandler, G. S. *J. Chem. Phys.* **1980**, *72*, 5639. Krishnan, R.; Binkley, J. S.; Seeger, R.; Pople, J. A. *J. Chem. Phys.* **1980**, *72*, 650.

(30) Andrae, D.; Haussermann, U.; Dolg, M.; Stoll, H.; Preuss, H. *Theor. Chim. Acta* **1990**, *77*, 123.

(31) Herzberg, G. *Molecular Spectra and Molecular Structure. II. Infrared and Raman Spectra of Polyatomic Molecules*; Van Nostrand Reinhold: New York, 1945.

(32) Milligan, D. W.; Jacox, M. E. *J. Chem. Phys.* **1971**, *55*, 3404. Hacaloglu, J.; Suzer, S.; Andrews, L. *J. Phys. Chem.* **1990**, *94*, 1759. Jacox, M. E. *J. Chem. Phys.* **1990**, *93*, 7622.

(33) Guillory, W. A.; Hunter, C. E. *J. Chem. Phys.* **1969**, *50*, 3516.

(34) Citra, A.; Chertihin, G. V.; Andrews, L.; Neurock, M. *J. Phys. Chem. A* **1997**, *101*, 3109.

(35) Klotzbucher, W.; Ozin, G. A. *J. Am. Chem. Soc.* **1975**, *97*, 2672. Andrews, L.; Citra, A.; Chertihin, G. V.; Bare, W. D.; Neurock, M. *J. Phys. Chem. A* **1998**, *102*, 2561.

(36) Bare W. D.; Citra, A.; Chertihin, G. V.; Andrews, L. *J. Phys. Chem. A* **1999**, *103*, 5456.

(37) Kundig, E. P.; Moskovits, M.; Ozin, G. A. *Can. J. Chem.* **1972**, *50*, 3587. Darling, J. H.; Ogden, J. S. *J. Chem. Soc., Dalton Trans.* **1973**, 1079. Liang, B. Y.; Zhou, M. F.; Andrews, L. *J. Phys. Chem. A* **2000**, *104*, 3905.

(38) Kasai, P. H.; Jones, P. M. *J. Phys. Chem*. **1985**, *89*, 1147. Kasai, P. H.; Jones, P. M. *J. Am. Chem. Soc.* **1985**, *107*, 6385.

(39) Kong, Q. Y.; Zeng, A. H.; Chen, M. H.; Xu, Q.; Zhou, M. F. *J. Phys. Chem. A* **2004**, *108*, 1531.

(40) Hildenbrand, D. L.; Lau, K. H. *Chem. Phys. Lett.* **2000**, *319*, 95.